Article

Construction of a nano biosensor for cyanide anion detection and its application in environmental and biological systems

Zhen-Zhen Dong, Chao Yang, Kasipandi Vellaisamy, Guodong Li, Chung-Hang Leung, and Dik-Lung Ma

ACS Sens., **Just Accepted Manuscript** • DOI: 10.1021/acssensors.7b00553 • Publication Date (Web): 26 Sep 2017

Construction of a nano biosensor for cyanide anion detection and its application in environmental and biological systems

Zhen-Zhen Dong[†], Chao Yang[‡], Kasipandi Vellaisamy[†], Guodong Li[‡], Chung-Hang Leung[*,‡] and Dik-Lung Ma[*,†]

[†]Department of Chemistry, Hong Kong Baptist University, Kowloon Tong, Hong Kong, China.

[‡]State Key Laboratory of Quality Research in Chinese Medicine, Institute of Chinese Medical Sciences, University of Macau, Macao, China.

KEYWORDS: Ag@Au core-shell nanoparticle; iridium(III) complex; cyanide; drinking water; cell imaging.

ABSTRACT: We have developed a Ag@Au core-shell nanoparticle (NP)/iridium(III) complex-based sensing platform for the sensitive luminescence "turn-on" sensing of cyanide ions, an acutely toxic pollutant. The assay is based on the quenching effect of Ag@Au NPs on the emission of complex **1**, but luminescence is restored after the addition of cyanide anions due to their ability to dissolve the Au shell. Our sensing platform exhibited a high sensitivity towards cyanide anions with a detection limit of 0.036 μM, and also showed high selectivity for cyanide over 10-fold excess amounts of other anions. The sensing platform was also successfully applied to monitor cyanide anions in drinking water and in living cells.

The cyanide anion can damage health and the environment due to its acute toxicity.[1-3] The cyanide anion inhibits the oxygen transport function in a_3 cytochrome by its strong interaction with the ferric ion of heme cofactors, causing harm to the central nervous and respiratory systems in mammals.[4-6] Large amounts of cyanide (around 1,400,000 tons per year) are produced in various fields of industry, including mining and electroplating.[7-8] Consequently, cyanide leakage and discharge can easily contaminate ground water and drinking water, which can induce lethality in aquatic organisms even at low concentration.[9] Therefore, a variety of strategies have been developed for the determination of cyanide, such as chromatography,[3, 10] electrochemistry,[11-12] colorimetry[13-14] and fluorescence.[15-17] Although some of these methods have good selectivity, their relatively low sensitivity limits their further practical application. Thus, a simple, selective and sensitive strategy is urgently needed for cyanide sensing.

Gold (Au) or silver (Ag) nanoparticles (NPs) are widely employed as colorimetric probes for cyanide sensing, for they can readily form Au/Ag-CN complexes in the presence of oxygen. A number of fluorescent probes based on Au NPs or Ag NPs have been reported that exhibited higher sensitivity than colorimetric assays.[18-23] Recently, bimetallic core-shell NPs have been explored to detect cyanide anion, with good simplicity, rapidity, high sensitivity and selectivity.[13] The surface plasmon resonance (SPR) of bimetallic core-shell nanoparticles could be tuned easily by the variation of the shell-to-core dimension ratio, leading to a clear spectral shift.[24-25]

Furthermore, iridium(III) complexes have drawn considerable attention owing to their unique photophysical properties in luminescence sensing, bioimaging and organic light-emitting devices[26-27]. Comparing with fluorescent organic dyes, iridium(III) complexes display various advantages, such as large Stokes shift, tunable luminescence emission and intensity, good photostability, long phosphorescence lifetime (~μs), high quantum yield and facile modification[28-29]. In particular, the long lifetimes of iridium(III) complexes allows time-resolved spectroscopy to be employed as a useful tool to eliminate adverse influences from autofluorescence in the biological environment. Thus, iridium(III) complexes are emerging as promising candidates for the applications of luminescence analysis and bioimaging[30-33].

Herein, we propose the first iridium(III) complex/Ag@Au core-shell NP-based "turn-on" luminescent platform for the detection of cyanide anion. In this work, we synthesized a novel iridium(III) complex with desirable optical and physical properties by adjusting

its C^N and N^N ligands. In the presence of Ag@Au core-shell NPs, the luminescence of the iridium(III) complex would be quenched effectively via the strong interaction between the iridium(III) complex and the Au shell of Ag@Au NPs. However, the addition of cyanide causes the detachment of the iridium(III) complex from the Au shell due to cyanide etching. As the iridium(III) complex interacts very weakly with the Ag core, this produces a strong luminescence enhancement even at very low concentration of cyanide. The use of the inert Au shell protects the Ag core from interactions with interferents such as iodide ions, increasing the stability and selectivity of the platform. We demonstrated the ability of our platform to detect cyanide in both drinking water and living cells.

EXPERIMENTAL SECTION

Materials and Apparatus. Cyanide standard solution (1000 μg/mL total cyanide), potassium hydroxide (KOH), trisodium citrate, coumarin 460 and sodium borohydride ($NaBH_4$) were purchased from J&K Scientific Limited Company (Beijing, China). Iridium chloride hydrate was obtained from Precious Metals Online (Australia). All the other reagents, unless specified, were bought from Sigma Aldrich (St. Louis, MO). Milli-Q ultrapure water was used for the preparation of all the aqueous solutions. Cyanide standard solution was stored at 4 ºC and diluted in KOH solution (pH = 10). All the chemicals were used as received without further purification.

All the luminescent emission spectra were collected by PTI QM-4/2005 Spectrometer. Lifetime was measured by PTI Time Master Model C-720 Spectrofluorometer. UV-Vis absorption spectra were recorded by Cary UV-300 (Double Beam) Spectrophotometer. Time-resolved emission spectra (TRES) experiments were investigated by Horiba Fluorescence Spectrometer. Transmission electron microscopy (TEM) images were taken by Tecnai G2 20 S-TWIN Transmission Electron Microscope.

Synthesis of complex 1. Complex **1** ($Ir(7\text{-}Clpq)_2(4,7\text{-}dmophen)$, where 7-Clpq = 7-chloro-2-phenylquinoline, 4,7-dmophen = 4,7-dimethoxy-1,10-phenanthroline) was synthesized following the procedure of our previous report with some modification.[34-36] In first step, the precursor $Ir_2(7\text{-}Clpq)_4Cl_2$ was prepared by the mixture of iridium chloride hydrate ($IrCl_3{\cdot}3H_2O$, 353 mg) and 7-Clpq (504 mg) in the solvent (2-ethoxyethanol:H_2O, 9:3, 12 mL). The obtained mixture was then stirred and heated at 130 ºC overnight. After cooling down to room temperature, water was added in the solution. The red solid was filtered and washed by water and ethyl ether to obtain the precursor. Subsequently, the precursor (71 mg) and 4,7-dmophen (27 mg) were added into 5 mL mixed solvent (dichloromethane:methanol, 1:1) and the mixture was refluxed overnight. And then it was cooled down to room temperature. Excess NH_4PF_6 was added and reaction solution was stirred over another 0.5 h. Then 5 mL dichloromethane was added and the solution washed by water three times and evaporated to give the solid. Finally, the solid was dissolved in acetone, following by the addition of diethyl ether to precipitate the product. And the precipitation was filtered under vacuum to obtain the desired product **1** (Fig. S1). The structure of complex **1** was confirmed by ^{1}H-NMR, ^{13}C-NMR (Fig. S2), high resolution mass spectrometry (HRMS, Fig. S3), elemental analysis and UV-Vis absorption (Fig. S4).

Fabrication of Ag@Au core-shell NPs. The Ag@Au NPs were fabricated according to the seed-growth method.[14] Briefly, 100 μL $AgNO_3$ (0.25 M) and 100 μL trisodium citrate (0.25 M) were mixed in ultrapure water (100 mL) with vigorous stirring at room temperature. 1 mL freshly prepared $NaBH_4$ solution (150 mM) was added quickly, which can reduce Ag^+ to form Ag NPs after 45 min. Next, 10 mL $NH_2OH{\cdot}HCl$ (6.25 mM) and 10 mL $HAuCl_4$ (0.0775 mM, 0.116 mM, 0.155 mM, 0.31 mM) were added dropwise to 12.5 mL of the obtained Ag NPs with continuous stirring for 1 h, generating Ag-core Au-shell (Ag@Au) nanoparticles with different thickness of Au shell (Au-1, Au-2, Au-3, Au-4).

Luminescent sensing of cyanide anion. In a typical experiment, the prepared Ag@Au NPs (150 μL), complex **1** (1 μM), pure water and solutions of cyanide anions at different concentrations were mixed in a total volume of 500 μL. After incubation for 10 min, the luminescence spectra in the range of 450–750 nm were measured using a PTI QM-4/2005 spectrometer.

Selectivity of the proposed platform. The selectivity of our proposed platform was evaluated using different anions at the indicated concentrations. After incubation of 10 min, the luminescence spectra were collected in the range of 450–750 nm.

Recovery experiments. The recovery assay was performed in the cyanide-spiked samples of drinking water under the same conditions of cyanide sensing in 2.4. The tap water was obtained in our lab directly, and the distilled water was bought from the supermarket without any purification. In addition, the values of recovery were calculated using the formula: Recovery (%) = (Found cyanide / Added cyanide) × 100%.

MTT assay. HeLa cells were seeded in 96-well plates at 8,000 cells per well and incubated overnight at 37 °C. Different concentrations of complex **1** were added to each well and the plates were incubated in a humidified CO_2 incubator for further 12 h at 37 °C. 100 μL of MTT (3-(4,5-dimethylthiazol-2-yl)-2,5-tetrazolium bromide) reagent (1 mg/mL) was added to each well. After 4 h incubation, the medium was replaced with 100 μL of dimethyl sulfoxide (DMSO) and the wells were incubated at 37 °C for 10 min with shaking. The cytotoxicity of complex **1** was exhibited as the percentage of absorbance in SpectraMax M5 microplate reader at a wavelength of 490 nm. The IC_{50} value was determined by the dose-dependence of the surviving cells.

Cell imaging. HeLa cells were cultured for 2 days in DMEM medium with 10% FBS and penicillin/streptomycin in a 5% CO_2 incubator at 37 °C. Before imaging, cells were seeded into a glass-bottomed dish (35 mm dish with 20 mm well). After 24 h, the cells were incubated with the indicated concentrations of complex **1** or Ag@Au NPs or cyanide for the indicated time and then washed with phosphate-buffered saline (PBS) three times. Luminescence imaging of complex **1** in cells was carried out using a Leica TCS SP8 confocal laser scanning microscope system. The excitation wavelength was 405 nm.

RESULTS AND DISCUSSION

Sensing Mechanism. The cyanide sensing mechanism of our proposed platform is described in Scheme 1. Complex **1** readily adsorbs onto the Au surface of Ag@Au NPs, leading to a decrease in luminescence signal with increasing concentration of NPs. This is presumed to occur via electrostatic interactions between the positive-charged complex **1** and the negative-charged Au shell, which is followed by energy transfer between the Ag@Au NPs and complex **1** leading to luminescence quenching. Ag@Au NPs (Au-2) had a broader absorption profile over the range of 300–800 nm (Fig. 1, curve d) compared to Ag NPs alone (Fig. 1, curve c). Importantly, the broad absorption spectrum of Ag@Au NPs could overlap with both the luminescence excitation and emission (Fig. 1, curves a and b) spectra of complex **1**, indicating that both the excited and emitted light of complex **1** could be adsorbed by Ag@Au NPs. Furthermore, the lifetime of complex **1** (4.416 μs) was the same in the absence or presence of Ag@Au NPs-**1**. From above all, the quenching mechanism is mainly contributed to static quenching effect (SQE) and inner filter effect (IFE).[37-38] The related static quenching constant was calculated to be 0.316 μM^{-1} (at 25 °C), according to the Stern-Volmer equation (see the Supporting Information).

However, upon the addition of cyanide, the Au shell of Ag@Au NPs becomes dissolved, causing the release of complex **1** from the surface of Ag@Au NPs. As the Ag core does not effectively quench the luminescence of complex **1**, the luminescence intensity of the system becomes restored significantly. The dissolution of the Au shell by cyanide is believed to proceed via the following reaction:[39]

$$4Au + 8CN^- + 2H_2O + O_2 \rightarrow 4[Au(CN)_2]^- + 4OH^-$$

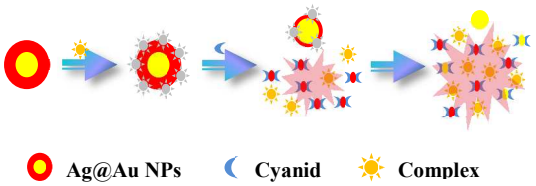

Scheme 1. The mechanism of the proposed platform for cyanide sensing.

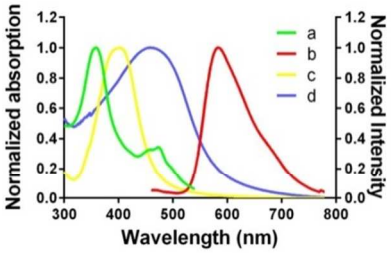

Fig. 1 a) Excitation and b) emission luminescence spectra of complex **1**; UV–Vis absorption spectra of c) Ag NPs (Ag core) and d) Ag@Au NPs (Au-2).

To demonstrate the feasibility of the proposed sensing principle, several control experiments were carried out. As shown in Fig. 2 (curves a and b), complex **1** becomes quenched by the addition of Ag@Au NPs. The corresponding absorption spectra are shown in Fig. S13). However, the addition of Ag NPs alone causes only a slight decrease in the luminescence of complex **1** (curve c). Importantly, the addition of cyanide causes an enhancement of the luminescence intensity of Ag@Au NPs-**1** (curve d) due to the aforementioned mechanism. However, cyanide alone had negligible effect on the luminescence of complex **1**, indicating that complex **1** does not interact with cyanide directly (curve e).

Optimization. Firstly, we investigated the influence of Ag@Au NPs with different Au shell thickness on complex **1** and cyanide sensing. As shown in Fig. S5, the absorption maximum of Ag NPs shifted from 408 nm to 529 nm with increasing Au shell thickness. Interestingly, the quenching interaction of Au shell and complex **1** became weaker with increasing thickness of the Au shell (Fig. S6). Finally, Au-2 exhibited the best performance for cyanide sensing (Fig. S7). Considering the above results, Au-2 was selected as the most suitable Au shell thickness for our sensing system. The core-shell structure of selected Ag@Au NPs could be recognized clearly by TEM image (Fig. S8).

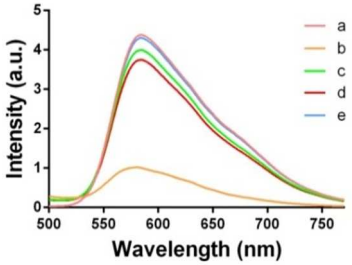

Fig. 2 The luminescence emission spectra of proposed sensing platform under different conditions in pure water. a) complex **1**; b) complex **1** + Ag@Au NPs; c) complex **1** + Ag NPs; d) complex **1** + Ag@Au NPs + cyanide; e) complex **1** + cyanide (complex **1**: 1 μM; cyanide: 100 μM).

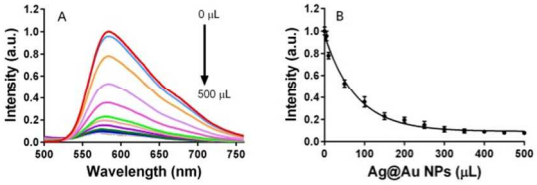

Fig. 3 Quenching effect of Ag@Au NPs towards complex **1** (1 μM).

In order to obtain better sensing performance, the concentration of Ag@Au NPs and reaction time were then optimized. Fig. 3 shows that the luminescence intensity of **1** gradually decreases with increasing concentrations of Ag@Au NPs and then reached a plateau at about 300 μL of added NPs (Fig. 3B). The absorption of complex **1** also increased with increasing concentrations of Ag@Au NPs (Fig. S14). To obtain a better luminescence response, 150 μL of Ag@Au NPs was used in subsequent experiments.

Next, the influence of incubation time on the luminescent signal was further investigated. The luminescence signal increased quickly after the addition of cyanide ions, and became steady after 5 min (Fig. S9). This suggests that the chemical reaction between cyanide ions and the Au shell is rapid. Therefore, the incubation time was set at 10 min to ensure the complete reaction of Ag@Au NPs and cyanide even at a low concentration of cyanide.

To examine the practicability of our proposed probe, its sensing ability towards cyanide was also investigated under various conditions of buffer systems, ionic strength and pH. The results showed that a similar signal-to-noise ratio could be achieved in the systems of pure water, PBS buffer (10 mM, pH = 7.4), Tris-HCl (10 mM, pH = 7.4) and HEPES buffer (10 mM, pH = 7.4) (Fig. S10). As for ionic strength, the proposed probe exhibited high sensing performance in the range of 0 to 20 mM PBS buffer, with a small decrease in sensing performance at 50 mM PBS due to the slight aggregation of Ag@Au NPs (Fig. S11). Meanwhile, the sensing ability was sensitive to pH values in the range of 5 to 10 (Fig. S12). The best luminescence signal could be observed at pH 7 or 8, while the luminescence enhancement was reduced at higher or

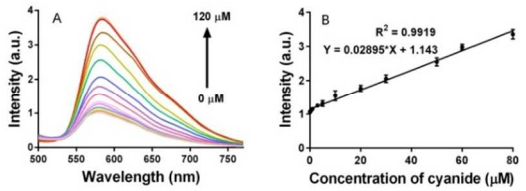

Fig. 4 The luminescence emission spectra of Ag@Au NPs-**1** in the presence of increasing cyanide concentrations (A) and corresponding linear relationship (B). F_0 is the luminescence intensity of Ag@Au NPs-**1**, F is the luminescence intensity in presence of cyanide.

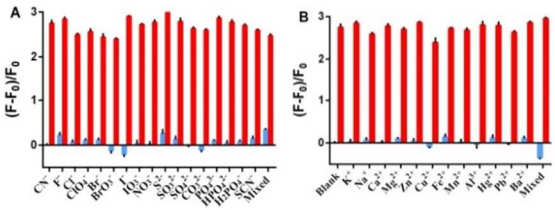

Fig. 5 The luminescence responses of Ag@Au NPs-**1** with (A) various anions (1 mM)) and cyanide (100 μM) or (B) metal ions (1 mM) in absence (blue bars) or in presence (red bar) of cyanide (100 μM). F_0 is the luminescence intensity of Ag@Au NPs-**1**, F is the luminescence intensity in presence of different anions.

lower pH values. Taken together, these results suggested that our probe is applicable for cyanide detection under a wide range of environmental and biological systems.

Sensitivity and selectivity. Under the optimized conditions, the analytical performance of our sensing strategy was evaluated at various concentrations of cyanide. The dissolution of Au shell could be observed clearly by the absorption changes (Fig. S15). The luminescence intensity of the system increased with the concentration of cyanide, as expected (Fig. 4A). A good linear relationship can be observed in the range of 0.05 to 80 μM cyanide (Fig. 4B). The assay had a detection limit of 0.036 μM (3σ, n = 9), which is more sensitive than most reported methods for cyanide determination using nanoparticles.[1, 13, 18-19, 40-45] Furthermore, our detection limit is much lower than the acceptable concentration of 1.9 μM of cyanide in drinking water according to the World Health Organization.[46] We also replace complex **1** by Rhodamine 6G to study the sensing ability for cyanide in the system. Rhodamine 6G could also be quenched gradually by increasing Ag@Au NPs (Fig. S16). However, luminescence recovery could be observed only at a concentration of 1 μM, and a linear relationship was only observed in the range of 1–50 μM (Fig. S17). The poorer performance of Rhodamine 6G compared to complex **1** could be attributed to the fact that Rhodamine 6G could be quenched not only by the Au shell, but also by the Ag core (Fig. S18). The results demonstrated the superior sensing ability of our proposed probe than organic dye.

To test the selectivity of the proposed platform for cyanide analysis, some other common anions (F^-, Cl^-, ClO_4^-, Br^-, BrO_3^-, I^-, IO_3^-, NO_3^-, S^{2-}, SO_3^{2-}, SO_4^{2-}, CO_3^{2-}, PO_4^{3-}, HPO_4^{2-}, $H_2PO_4^-$, SCN^-) and metal ions (K^+, Na^+, Ca^{2+}, Mg^{2+}, Zn^{2+}, Cu^{2+}, Fe^{2+}, Mn^{2+}, Al^{3+}, Hg^{2+}, Pb^{2+}, Ba^{2+}) were examined as interferents. The interferents almost had no effect on the luminescence signal of proposed sensing probe, even at a 10-fold excess concentration (1 mM) of interferents compared to cyanide (100 μM) in the presence of 16 mixed anions (Fig. 5A) or 12 mixed metal ions (Fig. 5B). This indicates that the assay is highly

selective for cyanide over the other anions and metal ions, which is presumed to be due to the unique ability of cyanide anions to dissolve Au. We further assessed the ability of our proposed platform for the determination of cyanide in drinking water. Recovery values of 98.0%–104.0% were obtained in spiked tap water and distilled water samples (Table 1), indicating the reliability and accuracy of the proposed method for sensing cyanide in real life samples.

Considering the long phosphorescence lifetime of complex **1** (Table S1), time-resolved spectroscopic experiments were performed in the presence of coumarin 460, a model for strong background fluorescence interference. Regardless of the presence of cyanide, the strong emission of coumarin could be observed at a wavelength of about 460 nm if the time gate was set to before the fluorescence decay time of coumarin, which could interfere with the luminescence signal of Ag@Au NPs-**1** (Fig. 6A). However, setting the time gate after the fluorescence decay time eliminates the signal from coumarin, so that only the phosphorescence of **1** is observed (Fig. 6B). This highlights the possibility of using the proposed system for sensing cyanide even in the presence of strong background fluorescence, via the use of time-resolved emission spectroscopy.

Table 1. Analytical results for the detection of cyanide in sparked drinking water samples.

Samples No.	Added (μM)	Found (μM)	Recovery (%)	RSD (%)
A1	1	1.06	106.0	3.7
A2	5	5.24	104.8	2.8
A3	10	9.79	97.9	5.2
A4	20	19.3	96.5	3.6
A5	50	51.2	102.4	3.3
B1	1	0.95	95.0	4.7
B2	5	4.9	98.0	2.2
B3	10	10.2	102.0	3.9
B4	20	20.7	103.5	5.6
B5	50	50.6	101.2	4.1

A: tap water; B: distilled water.

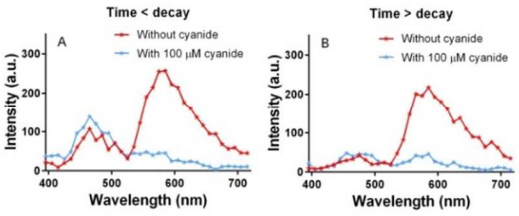

Fig. 6 Time-resolved emission spectra of proposed sensing platform in presence of coumarin. (complex **1**: 1 μM; Ag@Au NPs: 400 μL; coumarin: 0.5 μM; incubation time: 10 min)

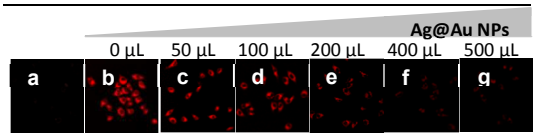

Fig. 7 Luminescence images of HeLa cells with incubation of: a) fresh medium; b–g) complex **1** + Ag@Au NPs for 2 h. (complex **1**: 1 μM)

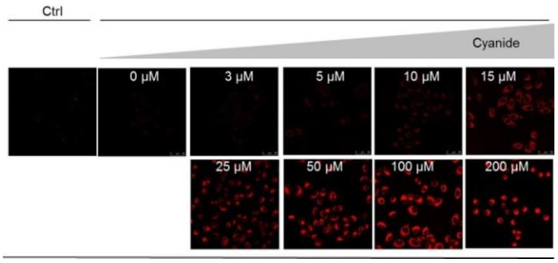

Fig. 8 Luminescence images of HeLa cells with incubation of fresh medium or Ag@Au NPs-**1** + cyanide anions. HeLa cells were pretreated with fresh medium or complex **1** + Ag@Au NPs for 1 h. The medium was replaced with cyanide for 1 h. (complex **1**: 1 μM; Ag@Au NPs: 400 μL)

Cell imaging. Due to the excellent performance of the sensing platform in aqueous solution, the feasibility of cyanide sensing was further demonstrated in living cells. The cytotoxicity of complex **1** towards HeLa cells was first studied by using an MTT assay. After incubation for 12 h, complex **1** inhibited the growth of HeLa cells with an IC_{50} value of 7.02 μM, which is much higher than the concentration of complex **1** used in the sensing experiments (1 μM) (Fig. S19). At 1 μM, complex **1** had no observable effect on the number and morphology of HeLa cells even after incubation for 6 h (Fig. S21).

Before cell imaging for cyanide, HeLa cells were pretreated with complex **1** (1 μM) for 1 h and then incubated with different concentrations of Ag@Au NPs for another 1 h. As shown in Fig. 7, the addition of various concentrations of Ag@Au NPs led to a significant decrease in the luminescence complex **1** in the HeLa cells. Remarkably, when HeLa cells were further treated with different concentrations of cyanide ions for 1 h, the luminescence signal was clearly restored. The application of cyanide detection in HeLa cells was examined from 0 μM to 200 μM. A luminescence signal can be observed even at a concentration of 10 μM, which can be regarded as the detection limit in HeLa cells (Fig. 8, Fig. S20). These results demonstrate that our sensing platform has the potential application for monitoring intracellular cyanide.

CONCLUSION

In summary, we developed a simple, rapid, sensitive turn-on luminescence sensing platform by employing Ag@Au NPs and the iridium(III) complex **1** for the

determination of cyanide anion. Furthermore, we have demonstrated the application of the system for sensing cyanide in drinking water samples (tap water and distilled water) and for bioimaging intracellular cyanide in HeLa cells. A low detection limit of 0.036 μM for cyanide was recorded and the system was also selective for cyanide over 10-fold excess of other anions. To the best of our knowledge, it is the first time that a Ag-core/Au-shell/iridium(III) complex sensing platform has been utilized for sensing and bioimaging cyanide.

ASSOCIATED CONTENT

Supporting Information.

Materials, detection methods, synthesis and characterization of complex, spectrum, and supporting experiments.

This material is available free of charge via the Internet at http://pubs.acs.org.

AUTHOR INFORMATION

Corresponding Author

* Dik-Lung Ma: edmondma@hkbu.edu.hk
* Chung-Hang Leung: duncanleung@umac.mo

Author Contributions

Zhen-Zhen Dong contributed to the main experiments and muniscript draft; Chao Yang completed the cell imaging and MTT assays; Kasipandi Vellaisamy helped to check the revisions; Guodong Li collected the characterization of iridium(III) complex; Chung-Hang Leung and Dik-Lung Ma proposed and instructed the project.

ACKNOWLEDGMENT

This work is supported by Hong Kong Baptist University (FRG2/16-17/007), the Health and Medical Research Fund (HMRF/14130522), the Research Grants Council (HKBU/12301115 and HKBU/201913), the National Natural Science Foundation of China (21575121), the Guangdong Province Natural Science Foundation (2015A030313816), the Hong Kong Baptist University Century Club Sponsorship Scheme 2016, the Interdisciplinary Research Matching Scheme (RC-IRMS/14-15/06), Innovation and Technology Fund (ITS/260/16FX), Matching Proof of Concept Fund (MPCF-001-2017/18), the Science and Technology Development Fund, Macao SAR (077/2016/A2 and 007/2014/AMJ), the University of Macau (MYRG2015-00137-ICMS-QRCM, MYRG2016-00151-ICMS-QRCM and MRG044/LCH/2015/ICMS), National Natural Science Foundation of China (21628502).

REFERENCES

1. Liu, J.; Liu, Y.; Liu, Q.; Li, C.; Sun, L.; Li, F., Iridium (III) complex-coated nanosystem for ratiometric upconversion luminescence bioimaging of cyanide anions. *J. Am. Chem. Soc.* **2011,** *133* (39), 15276-15279.

2. Panda, M.; Robinson, N. C., Kinetics and mechanism for the binding of HCN to cytochrome c oxidase. *Biochemistry* **1995,** *34* (31), 10009-10018.

3. Tomasulo, M.; Sortino, S.; White, A. J.; Raymo, F. M., Chromogenic oxazines for cyanide detection. *J. Org. Chem.* **2006,** *71* (2), 744-753.

4. Way, J. L., Cyanide intoxication and its mechanism of antagonism. *Annu. Rev. Pharmacol. Toxicol.* **1984,** *24* (1), 451-481.

5. Way, J. L.; Sylvester, D.; Morgan, R. L.; Isom, G. E.; Burrows, G. E.; Tamulinas, C. B.; Way, J. L., Recent perspectives on the toxicodynamic basis of cyanide antagonism. *Fundam. Appl. Toxicol.* **1984,** *4* (2), S231-S239.

6. Beasley, D.; Glass, W., Cyanide poisoning: pathophysiology and treatment recommendations. *Occ. Med.* **1998,** *48* (7), 427-431.

7. Ma, J.; Dasgupta, P. K., Recent developments in cyanide detection: A review. *Analytica Chimica Acta* **2010,** *673* (2), 117-125.

8. Liu, Y.; Ai, K.; Cheng, X.; Huo, L.; Lu, L., Gold - Nanocluster - Based Fluorescent Sensors for Highly Sensitive and Selective Detection of Cyanide in Water. *Adv. Funct. Mater.* **2010,** *20* (6), 951-956.

9. Shan, D.; Mousty, C.; Cosnier, S., Subnanomolar cyanide detection at polyphenol oxidase/clay biosensors. *Anal. Chem.* **2004,** *76* (1), 178-183.

10. Christison, T. T.; Rohrer, J. S., Direct determination of free cyanide in drinking water by ion chromatography with pulsed amperometric detection. *J. Chromatogr. A* **2007,** *1155* (1), 31-39.

11. Taheri, A.; Noroozifar, M.; Khorasani-Motlagh, M., Investigation of a new electrochemical cyanide sensor based on Ag nanoparticles embedded in a three-dimensional sol–gel. *J. Electroanal. Chem.* **2009,** *628* (1), 48-54.

12. Ding, G.; Zhou, H.; Xu, J.; Lu, X., Electrofluorochromic detection of cyanide anions using a benzothiadiazole-containing conjugated copolymer. *Chem. Commun.* **2014,** *50* (6), 655-657.

13. Zeng, J.-b.; Cao, Y.-y.; Chen, J.-j.; Wang, X.-d.; Yu, J.-f.; Yu, B.-b.; Yan, Z.-f.; Chen, X., Au@ Ag core/shell nanoparticles as colorimetric probes for cyanide sensing. *Nanoscale* **2014,** *6* (17), 9939-9943.

14. Li, Y.; Wang, Q.; Zhou, X.; Wen, C.-y.; Yu, J.; Han, X.; Li, X.; Yan, Z.-f.; Zeng, J., A convenient colorimetric method for sensitive and specific detection of cyanide using Ag@ Au core–shell nanoparticles. *Sens. Actuator B-Chem.* **2016,** *228*, 366-372.

15. Badugu, R.; Lakowicz, J. R.; Geddes, C. D., Enhanced fluorescence cyanide detection at physiologically lethal levels: reduced ICT-based signal transduction. *J. Am. Chem. Soc.* **2005,** *127* (10), 3635-3641.

16. Chang, H.-C.; Ho, J.-a. A., Gold nanocluster-assisted fluorescent detection for hydrogen peroxide and cholesterol based on the inner filter effect of gold nanoparticles. *Anal. Chem.* **2015,** *87* (20), 10362-10367.

17. Shang, L.; Dong, S., Design of fluorescent assays for cyanide and hydrogen peroxide based on the inner filter effect of metal nanoparticles. *Anal. Chem.* **2009,** *81* (4), 1465-1470.

18. Shang, L.; Jin, L.; Dong, S., Sensitive turn-on fluorescent detection of cyanide based on the dissolution of fluorophore functionalized gold nanoparticles. *Chemical Communications* **2009,** (21), 3077-3079.

19. Wei, S.-C.; Hsu, P.-H.; Lee, Y.-F.; Lin, Y.-W.; Huang, C.-C., Selective Detection of Iodide and Cyanide Anions Using Gold-

Nanoparticle-Based Fluorescent Probes. *ACS Applied Materials & Interfaces* **2012,** *4* (5), 2652-2658.

20. Wang, L.; Zheng, J.; Yang, S.; Wu, C.; Liu, C.; Xiao, Y.; Li, Y.; Qing, Z.; Yang, R., Two-photon sensing and imaging of endogenous biological cyanide in plant tissues using graphene quantum dot/gold nanoparticle conjugate. *ACS Appl. Mater. Interfaces* **2015,** *7* (34), 19509-19515.

21. Ensafi, A. A.; Kazemifard, N.; Rezaei, B., Label-free and turn-on fluorescent cyanide sensor based on CdTe quantum dots using silver nanoparticles. *RSC Advances* **2015,** *5* (50), 40088-40093.

22. Shiraishi, Y.; Nakamura, M.; Hayashi, N.; Hirai, T., Coumarin–Spiropyran Dyad with a Hydrogenated Pyran Moiety for Rapid, Selective, and Sensitive Fluorometric Detection of Cyanide Anion. *Anal. Chem.* **2016,** *88* (13), 6805-6811.

23. Qing, Z.; Hou, L.; Yang, L.; Zhu, L.; Yang, S.; Zheng, J.; Yang, R., A Reversible Nanolamp for Instantaneous Monitoring of Cyanide Based on an Elsner-Like Reaction. *Anal. Chem.* **2016,** *88* (19), 9759-9765.

24. Chuntonov, L.; Bar-Sadan, M.; Houben, L.; Haran, G., Correlating electron tomography and plasmon spectroscopy of single noble metal core–shell nanoparticles. *Nano Lett.* **2011,** *12* (1), 145-150.

25. Ma, Y.; Li, W.; Cho, E. C.; Li, Z.; Yu, T.; Zeng, J.; Xie, Z.; Xia, Y., Au@ Ag core-shell nanocubes with finely tuned and well-controlled sizes, shell thicknesses, and optical properties. *ACS nano* **2010,** *4* (11), 6725.

26. Liu, Z.; Guan, M.; Bian, Z.; Nie, D.; Gong, Z.; Li, Z.; Huang, C., Red Phosphorescent Iridium Complex Containing Carbazole - Functionalized β - Diketonate for Highly Efficient Nondoped Organic Light - Emitting Diodes. *Adv. Funct. Mater.* **2006,** *16* (11), 1441-1448.

27. Sun, C.-Y.; Wang, X.-L.; Zhang, X.; Qin, C.; Li, P.; Su, Z.-M.; Zhu, D.-X.; Shan, G.-G.; Shao, K.-Z.; Wu, H., Efficient and tunable white-light emission of metal–organic frameworks by iridium-complex encapsulation. *Nat. Commun.* **2013,** *4*.

28. Chen, F.-C.; Yang, Y.; Thompson, M. E.; Kido, J., High-performance polymer light-emitting diodes doped with a red phosphorescent iridium complex. *Appl. Phys. Lett.* **2002,** *80* (13), 2308-2310.

29. You, Y.; Park, S. Y., Inter-ligand energy transfer and related emission change in the cyclometalated heteroleptic iridium complex: facile and efficient color tuning over the whole visible range by the ancillary ligand structure. *J. Am. Chem. Soc.* **2005,** *127* (36), 12438-12439.

30. Leung, K.-H.; He, H.-Z.; Wang, W.; Zhong, H.-J.; Chan, D. S.-H.; Leung, C.-H.; Ma, D.-L., Label-free luminescent switch-on detection of endonuclease IV activity using a G-quadruplex-selective iridium (III) complex. *ACS Appl. Mater. Interfaces* **2013,** *5* (23), 12249-12253.

31. Liu, C.; Yang, C.; Lu, L.; Wang, W.; Tan, W.; Leung, C.-H.; Ma, D.-L., Luminescent iridium (III) complexes as COX-2-specific imaging agents in cancer cells. *Chem. Commun.* **2017,** *53* (19), 2822-2825.

32. Wang, W.; Yang, C.; Lin, S.; Vellaisamy, K.; Li, G.; Tan, W.; Leung, C. H.; Ma, D. L., First Synthesis of an Oridonin - Conjugated Iridium (III) Complex for the Intracellular Tracking of NF - κ B in Living Cells. *Chem. Eur. J.* **2017,** *23* (20), 4929-4935.

33. Ko, C.-N.; Yang, C.; Lin, S.; Li, S.; Dong, Z.; Liu, J.; Lee, S. M.-Y.; Leung, C.-H.; Ma, D.-L., A long-lived phosphorescence iridium (III) complex as a switch on-off-on probe for live zebrafish monitoring of endogenous sulfide generation. *Biosens. Bioelectron.* **2017,** *94*, 575-583.

34. Lin, S.; Lu, L.; Kang, T.-S.; Mergny, J.-L.; Leung, C.-H.; Ma, D.-L., Interaction of an Iridium (III) Complex with G-Quadruplex DNA and Its Application in Luminescent Switch-On Detection of Siglec-5. *Anal. Chem.* **2016,** *88* (20), 10290-10295.

35. Wang, M.; Wang, W.; Kang, T.-S.; Leung, C.-H.; Ma, D.-L., Development of an Iridium (III) complex as a G-quadruplex probe and its application for the G-quadruplex-based luminescent detection of picomolar insulin. *Anal. Chem.* **2015,** *88* (1), 981-987.

36. Dong, Z.-Z.; Lu, L.; Ko, C.-N.; Yang, C.; Li, S.; Lee, M.-Y.; Leung, C.-H.; Ma, D.-L., A MnO 2 nanosheet-assisted GSH detection platform using an iridium (iii) complex as a switch-on luminescent probe. *Nanoscale* **2017**.

37. Darbha, G. K.; Ray, A.; Ray, P. C., Gold nanoparticle-based miniaturized nanomaterial surface energy transfer probe for rapid and ultrasensitive detection of mercury in soil, water, and fish. *Acs Nano* **2007,** *1* (3), 208-214.

38. Yuan, P.; Walt, D. R., Calculation for fluorescence modulation by absorbing species and its application to measurements using optical fibers. *Anal. Chem.* **1987,** *59* (19), 2391-2394.

39. Hiskey, J.; Sanchez, V., Mechanistic and kinetic aspects of silver dissolution in cyanide solutions. *J. Appl. Electrochem.* **1990,** *20* (3), 479-487.

40. Kim, M. H.; Kim, S.; Jang, H. H.; Yi, S.; Seo, S. H.; Han, M. S., A gold nanoparticle-based colorimetric sensing ensemble for the colorimetric detection of cyanide ions in aqueous solution. *Tetrahedron Lett.* **2010,** *51* (36), 4712-4716.

41. Hajizadeh, S.; Farhadi, K.; Forough, M.; Sabzi, R. E., Silver nanoparticles as a cyanide colorimetric sensor in aqueous media. *Anal. Methods* **2011,** *3* (11), 2599-2603.

42. Liu, C.-Y.; Tseng, W.-L., Colorimetric assay for cyanide and cyanogenic glycoside using polysorbate 40-stabilized gold nanoparticles. *Chem. Commun.* **2011,** *47* (9), 2550-2552.

43. Radhakumary, C.; Sreenivasan, K., Rapid and highly selective dipchecking for cyanide ions in aqueous media. *Analyst* **2012,** *137* (22), 5387-5391.

44. Zhai, Y.; Jin, L.; Wang, P.; Dong, S., Dual-functional Au–Fe 3 O 4 dumbbell nanoparticles for sensitive and selective turn-on fluorescent detection of cyanide based on the inner filter effect. *Chem. Commun.* **2011,** *47* (29), 8268-8270.

45. Lou, X.; Zeng, Q.; Zhang, Y.; Wan, Z.; Qin, J.; Li, Z., Functionalized polyacetylenes with strong luminescence:"turn-on" fluorescent detection of cyanide based on the dissolution of gold nanoparticles and its application in real samples. *J. Mater. Chem.* **2012,** *22* (12), 5581-5586.

46. Organization, W. H., *Guidelines for drinking-water quality*. World Health Organization: **2004**; Vol. 1.

Table of Contents

We have developed a Ag@Au core-shell nanoparticle (NP)/iridium(III) complex-based sensing platform for the sensitive luminescence "turn-on" sensing of cyanide ions.